BIOCHEMISTRY
including biophysical chemistry & molecular biology

ARTICLE

pubs.acs.org/biochemistry

Accommodating a Nonconservative Internal Mutation by Water-Mediated Hydrogen Bonding between β-Sheet Strands: A Comparison of Human and Rat Type B (Mitochondrial) Cytochrome b_5

Sudharsan Parthasarathy,[†] Adriana Altuve,[‡] Simon Terzyan,[§] Xuejun Zhang,[§] Krzysztof Kuczera,[†,‡] Mario Rivera,[‡] and David R. Benson[*,†,‡]

[†]Department of Molecular Biosciences, University of Kansas, Lawrence, Kansas 66045, United States

[‡]Department of Chemistry, University of Kansas, Lawrence, Kansas 66045, United States

[§]Crystallography Program, Oklahoma Medical Research Foundation, Oklahoma City, Oklahoma 73104-5097, United States

Supporting Information

ABSTRACT: Mammalian type B (mitochondrial) b_5 cytochromes exhibit greater amino acid sequence diversity than their type A (microsomal) counterparts, as exemplified by the type B proteins from human (hCYB5B) and rat (rCYB5B). The comparison of X-ray crystal structures of hCYB5B and rCYB5B reported herein reveals a striking difference in packing involving the five-strand β-sheet, which can be attributed to fully buried residue 21 in strand β4. The greater bulk of Leu21 in hCYB5B in comparison to that of Thr21 in rCYB5B results in a substantial displacement of the first two residues in β5, and consequent loss of two of the three hydrogen bonds between β5 and β4. Hydrogen bonding between the residues is instead mediated by two well-ordered, fully buried water molecules. In a 10 ns molecular dynamics simulation, one of the buried water molecules in the hCYB5B structure exchanged readily with solvent via intermediates having three water molecules sandwiched between β4 and β5. When the buried water molecules were removed prior to a second 10 ns simulation, β4 and β5 formed persistent hydrogen bonds identical to those in rCYB5B, but the Leu21 side chain was forced to adopt a rarely observed conformation. Despite the apparently greater ease of access of water to the interior of hCYB5B than of rCYB5B suggested by these observations, the two proteins exhibit virtually identical stability, dynamic, and redox properties. The results provide new insight into the factors stabilizing the cytochrome b_5 fold.

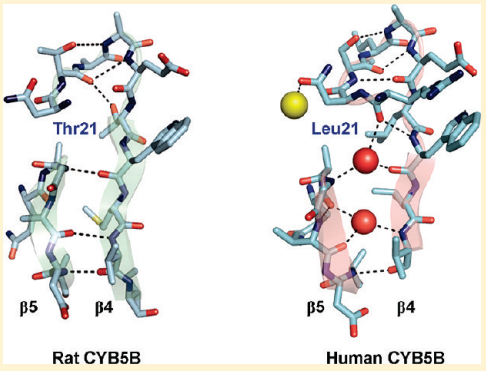

Two genes in vertebrates encode tail-anchored isoforms of the electron transfer heme protein cytochrome b_5.[1,2] One isoform resides in the endoplasmic reticulum and has long been known as microsomal (Mc) cytochrome b_5 but now is designated as type A cytochrome b_5 (CYB5A). CYB5A provides electrons to a wide array of proteins, including fatty acid desaturases and P450 cytochromes.[3−6] The other isoform is associated with the outer mitochondrial membrane and was formerly termed OM cytochrome b_5 but is now designated as type B cytochrome b_5 (CYB5B). Although relatively little is known about the physiological roles of CYB5B,[7,8] recent studies have shown that it is constitutively overexpressed in malignant lymphomas.[9]

CYB5A and CYB5B contain a compact hydrophilic N-terminal heme-binding domain and a hydrophobic C-terminal membrane-anchoring domain. The heme-binding domain folds independently and is more soluble than the full-length protein. As a consequence, structural studies of cytochrome b_5 have focused on fragments containing the heme-binding domain. The only X-ray crystal structures published to date for vertebrate cytochrome b_5 heme-binding domains are those for bovine CYB5A (bCYB5A)[10,11] and rat CYB5B (rCYB5B).[12] The structure of the 86-residue bCYB5A lipase fragment was the first to be reported[13,14] and was ultimately refined to 1.5 Å (PDB entry 1CYO).[10] A crystal structure of the 82-residue tryptic fragment of bCYB5A is also available (PDB entry 1EHB).[11] As has been our practice, we will utilize the numbering system adopted for the lipase fragment (Figure 1) in this work.

The elements of secondary structure in CYB5A and CYB5B fall in the order β1-α1-β4-β3-α2-α3-β5-α4-α5-β2-α6. The protein has been described as comprising two hydrophobic cores separated by a five-strand β-sheet.[15] As highlighted for bCYB5A in Figure 2, core 1 contains heme surrounded by helices α2−α5. Heme iron is ligated by histidine residues 39 and 63, each residing in a loop separating a pair of core 1 helices. His39 is the first residue in the HPGG loop motif that lies between α2 and α3 and is characteristic of all known eukaryotic members of the

Received: March 29, 2011
Revised: May 12, 2011
Published: May 16, 2011

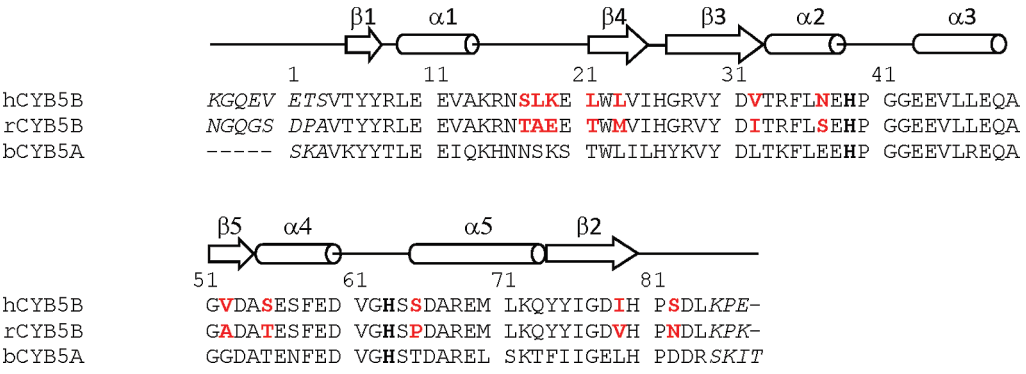

Figure 1. Alignment of the polypeptide fragments used for determining the X-ray crystal structures of hCYB5B and rCYB5B reported herein, and of the lipase fragment of bCYB5A against which they are compared. The numbering follows the scheme introduced by Mathews for the bCYB5A lipase fragment.[15] β-Sheet strands are represented as arrows and helices as cylinders. Heme-ligating histidine residues are shown in bold. Residues differing between hCYB5B and rCYB5B are colored red. Italicized residues are not involved in specific packing interactions and are either poorly resolved or not observed.

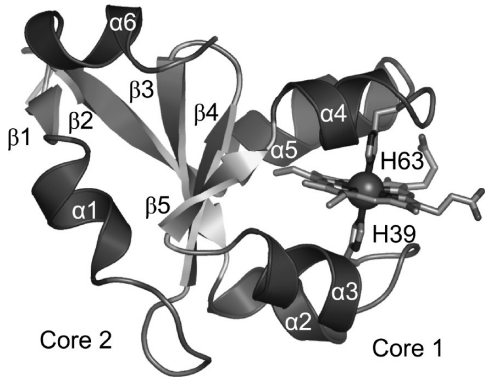

Figure 2. Cartoon representation of the X-ray crystal structure of the bCYB5A lipase fragment[10] (PDB entry 1CYO), highlighting secondary structure elements, heme and ligands His39 and His63, and hydrophobic cores 1 and 2. The image was generated using PyMol version 0.99 (http://www.pymol.org/).

cytochrome b_5 superfamily. The loop containing His63 is located between α4 and α5 and in all known examples of CYB5A and CYB5B has the sequence VGHS. Core 2 contains helix α1 and a C-terminal 3_{10}-helix designated α6. Cores 1 and 2 are separated by a five-strand β-sheet, although residues 51−54 that comprise one of the edge strands (β5) lie within the region of the polypeptide that defines the four-helix bundle surrounding heme (between α3 and α4). The secondary structure elements described above are maintained in solution, as evidenced by published structures determined by nuclear magnetic resonance (NMR) for bovine,[16,17] rat,[18] rabbit,[19] and human[20] CYB5A.

At the time the rCYB5B X-ray crystal structure was determined (PDB entry 1B5M),[12] no other type B cytochrome b_5 had been identified. In contrast, amino acid sequences for several type A b_5 cytochromes had been reported and shown to exhibit an extremely high degree of sequence homology. It was discovered that rCYB5B differs from CYB5A in being considerably more stable[21] and having a significantly more negative redox potential.[22] The greater stability has been shown to result, in part, from a more extensive network of hydrophobic interactions at the base of its heme-binding pocket.[23−27] The source of the more negative redox potential of CYB5B is an area of active investigation in our laboratories.

The second CYB5B to be discovered, from human (hCYB5B), was predicted to have a hydrophobic patch even more extensive than that in rCYB5B on the basis of an amino acid sequence comparison.[28] It was shown to be similar in stability to rCYB5B and likewise to have a redox potential more negative than those reported for CYB5A, albeit less negative (−40 mV vs SHE) than that reported for rCYB5B (−102 mV vs SHE). These observations led us to propose that more extensive hydrophobic packing, greater stability, and more negative redox potentials are factors that distinguish all CYB5B proteins from their CYB5A counterparts.[28] The increasing availability of CYB5A and CYB5B amino acid sequences has strengthened these hypotheses.[29] It has also made us aware that CYB5B exhibits amino acid sequence diversity at positions that are invariant or highly conserved in CYB5A (see Figure S1 of the Supporting Information), which is likely to be manifested in variations in surface properties and internal packing. Because rCYB5B and hCYB5B are reflective of this diversity, we were motivated to obtain an X-ray crystal structure of the latter, which has been determined to 1.45 Å. We have also obtained a new crystal structure of rCYB5B having a resolution (2.0 Å) higher than the previously reported one (2.7 Å).[12] Amino acid sequences of the rCYB5B and hCYB5B fragments used to generate the crystal structures described here are aligned with the corresponding sequence of the bCYB5A lipase fragment in Figure 1. The 12 residues that differ between hCYB5B and rCYB5B are highlighted in red in Figure 1.

Herein, we show that the hCYB5B structure differs from the rCYB5B structure in containing two well-resolved and completely buried water molecules mediating hydrogen bonding between β-sheet strands β4 and β5. The difference could be traced to fully buried residue 21 in β4, which is much bulkier in hCYB5B (Leu) than in rCYB5B (Thr). The results provide new insight into the factors stabilizing the cytochrome b_5 fold, in particular the role of invariant residue Ala54 (in β5). We also show that the redox potentials of hCYB5B and rCYB5B are more similar than previously reported.

MATERIALS AND METHODS

Proteins. Expression systems for rCYB5B,[30] hCYB5B,[28] and bCYB5A[24] used in the studies reported herein have been described previously. All proteins were expressed in *Escherichia coli* BL21(DE3) cells. rCYB5B and hCYB5B used in the

crystallographic studies were expressed and purified using previously reported methods.[28,30] Proteins used in the redox potentiometry experiments were expressed and purified as follows. Transformed cells were grown in 1 L of LB medium at 37 °C, with 200 rpm shaking, until OD_{600} reached ~0.7. Protein expression was induced with 1 mM IPTG (final concentration), and cells were grown for an additional 7 h at 25 °C, with 150 rpm shaking. All subsequent steps were performed at 4 °C unless otherwise noted. Cells were harvested by centrifugation (5000 rpm, JA-10 rotor, Beckman-Coulter) and lysed by being frozen and thawed and sonicated in lysis buffer [20 mM Tris (pH 7.0) and 50 mM PMSF]. Cell debris was separated by centrifugation (20000 rpm for 1 h, JA-20 rotor, Beckman-Coulter).

A hemin solution (5 mg/mL in DMSO) was slowly added to the crude cell lysate at room temperature until A_{412} reached a maximum. Excess hemin was first removed by centrifugation (20000 rpm for 2 h, JA-20 rotor, Beckman-Coulter), and the filtered supernatant was loaded onto a Q-Sepharose column (GE Life Sciences). The protein was eluted using a linear gradient (0 to 1 M) of NaCl in 20 mM Tris-HCl (pH 7.0). Red-colored fractions were pooled and subjected to further purification using a Phenyl-Sepharose column (GE Life Sciences) under a reverse gradient (1 to 0 M NaCl) in the buffer mentioned above. Final purification was performed on pooled protein-containing fractions using a Superdex 200 gel filtration column (GE Life Sciences) with the same buffer. All purifications were performed on an AKTA- FPLC purification system (GE Life Sciences). Purity was confirmed by native gel electrophoresis that also confirmed the absence of any apoprotein. All proteins were exchanged into 50 mM sodium phosphate buffer (pH 7.0) using an Amicon protein concentration system (Millipore Corp.).

Crystallization and Structure Solution. Thick rectangular crystals of hCYB5B appeared from hanging drops containing equal amounts of protein at a concentration of 20 mg/mL [in 20 mM Tris-HCl (pH 7)] and a reservoir solution composed of 30% PEG8K, 0.1 M Hepes (pH 6.8), and 0.2 M magnesium acetate. Drops were equilibrated against the reservoir solution at 5 °C. Before the crystal was cryocooled in the 100 K gas stream of nitrogen, it was equilibrated against a solution similar to the reservoir solution but containing 36% PEG8K. X-ray diffraction data were collected to 1.45 Å resolution at the Cornell High Energy Synchrotron Source (CHESS) F1 station (Cornell University, Ithaca, NY), tuned to 0.976 Å X-ray wavelength, using an ADSC Quantum 4 CCD detector system.

High- and low-resolution data sets were collected using crystal −detector distances of 125 and 200 mm and exposure times of 60 and 20 s, respectively. Data were processed with the HKL2000 program suite.[31] The crystal belongs to space group $P2_1$ and contains two molecules of hCYB5B per asymmetric unit. The position and orientation of the two molecules in the unit cell of the crystal were determined by molecular replacement with AMoRe[32] using our structure of the quintuple mutant of rCYB5B (PDB entry 1LJ0),[24] without the heme group, as the search model. Initially, several cycles of refinement were conducted with the CNS program suite.[33] One cycle of simulated annealing with the slowcool protocol from 5000 K was followed by several cycles of positional and isotropic individual temperature factor refinement with bulk solvent correction and anisotropic overall B factor refinement at the full resolution range. Manual model building was conducted with the interactive graphics program TURBO-FRODO[34] using $2|F_o| - |F_c|$ and $|F_o| - |F_c|$ difference Fourier maps. Water molecules were added to the structure automatically using the water-pick program of CNS.

When the refinement converged, some side chains (Ile79 of molecule A and Glu−2 and Ser57 of molecule B) were modeled in two alternative positions. Heme in both molecules was also resolved in two alternative orientations, differing by a 180° rotation about the $\alpha-\gamma$-meso axis. Each population exhibits 50% occupancy, consistent with the 1:1 ratio present in the crystallization sample. On the basis of coordination and electron density, four water molecules were replaced with two Mg^{2+} ions and two SO_4^- groups. The structure of the molecule refined with CNS contained 1458 protein atoms, 86 heme atoms, two Mg ions, and two SO_4 groups and had R_{work} and R_{free} values of 0.177 and 0.215, respectively. Final refinement of the structure with the full data set (working and free data sets combined) and anisotropic individual temperature factors was conducted with REFMAC[35] and resulted in a crystallographic R factor of 0.199.

Crystal growth conditions for rCYB5B were similar to those for the human protein. Data were collected at room temperature on a four-circle Siemens diffractometer equipped with a multiwire area detector. The reflections were indexed, integrated, and scaled using SAIDE and SAINT.[36] The crystal belongs to space group $P2_12_12_1$ and contains two molecules of rCYB5B per asymmetric unit. Because this crystal form is different from the previously reported one [$P4_32_12$ with one molecule per asymmetric unit (PDB entry 1B5M)],[12] its structure was again determined by molecular replacement. Initially, the structure was refined using TNT.[37] Final stages of refinement were conducted using the CNS suite.[33] For model building of both proteins, TURBO-FRODO[34] and COOT[38] were used. Although the rCYB5B sample used for crystallization contained a 1:1 ratio of heme orientations, we were unable to resolve the isomers. The coordinates for rCYB5B (PDB entry 3MUS) and hCYB5B (PDB entry 3NER) have been deposited in the Protein Data Bank. Statistics for both structures are listed in Table S1 of the Supporting Information.

Molecular Dynamics Simulations. Ten nanosecond molecular dynamics (MD) simulations were performed on hCYB5B and rCYB5B using CHARMM (version 33a1[39]). All atom topology and parameter sets (version 22) along with dihedral cross-term corrections (CMAP) were used in all calculations.[40] X-ray crystal structures of rCYB5B and hCYB5B were used as the starting structures for the MD simulations. Missing hydrogen atoms were added to complete all atom models using the HBUILD module of CHARMM.[41] The proteins were then subjected to a gradual energy minimization in vacuum to prevent any atomic clashes. Energy-minimized proteins were neutralized by the addition of Na^+ and Cl^- counterions to an ionic strength of 0.15 M. Counterions were added using the Solvator module in CHARMM-GUI.[42]

The entire system (protein and counterions) was immersed in a truncated octahedral water cell, built by cutting off corners from a cube with an edge length of 70 Å. Water molecules overlapping the protein and counterions were removed, yielding the final simulation system. Water molecules and counterions were subjected to an initial equilibration for 0.1 ns in the presence of a fixed solute. A final equilibration for 0.1 ns was performed on the whole system before the trajectory production stage. Equilibration and MD simulations were performed at a constant temperature (300 K) and pressure (1 atm). The Hoover thermostat method[43] was used to maintain a constant temperature, and the Langevin piston method[44] was used to maintain a constant

temperature. The IMAGE facility in CHARMM was used to generate periodic boundary conditions and to solvate the system. The particle-mesh Ewald method[45] was used to expand long-range forces in the calculation of electrostatic interactions. The Ewald parameter, κ, was set to 0.34 $Å^{-1}$; the grid spacing parameter, L, was set to 64, and the cutoff distance was set to 12 Å. Bonds involving hydrogen atoms in the system were kept fixed using the SHAKE algorithm.[46] A 2 fs time step was used in association with the Leapfrog integrator.[43] Every 250 steps (0.5 ps), coordinates were saved, yielding a total of 20000 coordinate frames for subsequent analysis. Before analysis, the trajectory structures of the solute were transformed by centering in the solvent box and overlay of the peptide backbone atoms on the starting structure. This allowed the investigation of internal protein structure fluctuations via removal of overall rotational and translational motions. The solvent accessible surface area of the CYB5Bs was calculated using Lee and Richards's algorithm[47] with a probe radius of 1.6 Å. Visualization of trajectories was performed using the molecular graphics packages VMD[48] and PyMol (http://www.pymol.org).

Redox Potentiometry. Redox potentiometry experiments were conducted using a modification of a previously described protocol.[28] The redox cell consisted of a 5 mL beaker with a stir bar and a calomel electrode [241 mV vs SHE (Radiometer Analytical)] connected to a pH meter operating in voltage mode. Absorption spectra were recorded using a USB 2000 fiber optic spectrophotometer outfitted with a dip probe (Ocean Optics, Dunedin, FL). The entire setup was housed under an N_2/H_2 atmosphere (1−2% H_2) in an anaerobic glovebox (Coy Laboratories, Grass Lake, MI). All experiments were conducted in 50 mM sodium phosphate buffer (pH 7.0) (ionic strength of 0.11 M) with a protein concentration of 10 μM and each redox mediator at a concentration of 1 μM. For reductive or oxidative titrations, appropriate volumes of a sodium dithionite stock solution (4 mM) or a potassium ferricyanide stock solution (1 mM), respectively, were added using a Hamilton microsyringe. Changes in oxidation state of the heme were monitored using the α band at 557 nm, and the voltage was recorded after equilibrium had been achieved (typically 15 min). The data were fit to a one-electron Nernst equation using Igor Pro (version 4.0, Wavemetrics Inc.).

The redox mediators used, with their standard potentials versus SHE, were methyl viologen (−430 mV), benzyl viologen (−311 mV), anthraquinone-2-sulfonic acid (−225 mV), anthraquinone-2,6-disulfonic acid sodium salt (−184 mV), 2-hydroxy-1,4-naphthoquinone (−152 mV), 2,5-dihydroxy-1,4-benzoquinone (−60 mV), 5,8-dihydroxy-1,4-naphthoquinone (−50 mV), pyocyanin (−34 mV), duroquinone (5 mV), 5-hydroxy-1,4-naphthoquinone (33 mV), 1,4-naphthoquinone (50 mV), phenazine methosulfate (80 mV), 2,6-dimethylbenzoquinone (115 mV), 1,2-naphthoquinone (157 mV), 2-methyl-1,4-benzoquinone (175 mV), and 1,2-naphthoquinone-4-sulfonic acid (210 mV). The electrode was calibrated using a suspension of quinhydrone in 50 mM sodium phosphate buffer (pH 7.0) (280 mV vs SHE). For rCYB5B and hCYB5B, three reductive titrations were performed as described above. For bCYB5A, two reductive titrations were performed along with one oxidative titration. Table 2 reports the average and standard deviation from the three independent runs. All redox mediators were purchased from Sigma-Aldrich (St. Louis, MO), except for pyocyanin (Cayman Chemical, Ann Arbor, MI).

RESULTS AND DISCUSSION

Comparison of the rCYB5B and hCYB5B Crystal Structures. The previously published 2.7 Å structure of rCYB5B contained one molecule in the asymmetric unit,[12] but in the new higher-resolution structure, there are two. The 1.45 Å structure of hCYB5B also contains two molecules in the asymmetric unit (space group $P2_1$), but with different relative orientations compared to that of rCYB5B (space group $P2_12_12_1$). The following comparison of the hCYB5B and rCYB5B structures refers to molecule A in the asymmetric unit of each.

The plot of average main chain crystallographic temperature factors (B factors) for the hCYB5B polypeptide in Figure S2 of the Supporting Information indicates that the β-sheet strands (average B factor of 12.5) are less mobile than the more highly solvent-exposed α-helices (average B factor of 17.2), consistent with solution NMR studies of both type A[18,49] and type B[49] b_5 cytochromes. Note that we have followed the generally accepted convention of defining the β-sheet strands by the order in which they appear in the β-sheet, as in the original papers describing the crystal structure of bCYB5A (Figures 1 and 2),[13−15] rather than by their order within the protein sequence as in the paper reporting refinement of the bCYB5A structure.[10] The first (β1) and last (β5) strands in the β-sheet have solvent-exposed edges and are very short (residues 5−7 and 51−54, respectively).

The root-mean-square deviation (rmsd) plot in Figure S3A of the Supporting Information shows that bCYB5A and rCYB5B have virtually identical folds (average Cα rmsd of 0.56 Å), consistent with a previous analysis utilizing the 2.7 Å structure of rCYB5B.[12] A significant difference is observed in the folds of rCYB5A and hCYB5B, however, most notably for residues 50−53 (Figure S3B of the Supporting Information). Not surprisingly, smaller average rmsd Cα differences are observed for the two molecules in the rCYB5B (0.23 Å) and hCYB5B (0.29 Å) asymmetric units.

Hydrophobic Clusters. Studies in our laboratories have revealed that rCYB5B and hCYB5B are considerably more stable than known examples of CYB5A. Mutagenesis studies with rCYB5B have shown that this is due, in large measure, to a more extensive network of hydrophobic packing interactions involving heme and the side chains of residues at the core 1−core 2 interface.[23,24,26,50] The hydrophobic cluster in rCYB5B begins at the top of the protein as represented in Figure 3A, with van der Waals contact between the solvent-exposed side chains of Ala18 and Leu47, and ends at the bottom of the protein with the partially solvent-exposed side chain of Leu71. Residues in this network with side chains engaging in hydrophobic interactions with heme are Met23, Ile25, Ile32, Leu71, and Phe58. The corresponding region in all reported examples of mammalian CYB5A is less hydrophobic, largely because of the presence of residues with solvent-exposed polar side chains at positions 18 (Ser), 47 (Arg), and 71 (Ser). Tables S2 and S3 (Supporting Information) show that there is considerably greater variability among the residues comprising the hydrophobic cluster in mammalian CYB5B than among the corresponding residues in CYB5A.

In our report showing that hCYB5B exhibits stability properties similar to those of rCYB5B,[28] we predicted that it would have a similar hydrophobic cluster as well because it differs at only three amino acids in that region: 18 (Leu rather than Ala), 23 (Leu rather than Met), and 32 (Val rather than Ile). The latter two differences involve residues with fully buried side chains and

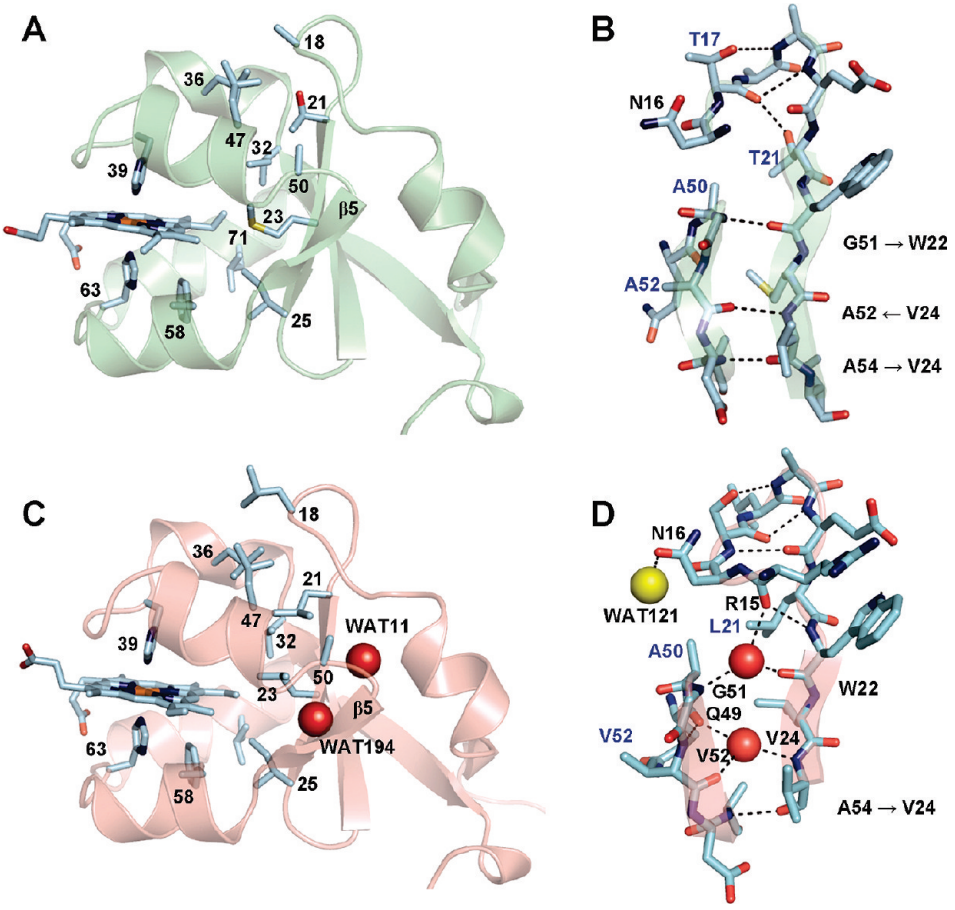

Figure 3. Comparison of the crystal structures of rCYB5B (top) and hCYB5B (bottom), highlighting differences in their hydrophobic clusters (A and C) and hydrogen bonding interactions between β-sheet strands β4 and β5 (B and D). Buried water molecules WAT11 and WAT194 in the hCYB5B structure are shown as red spheres, and WAT121 is shown as a yellow sphere. Images were generated using PyMol version 0.99 (http://www.pymol.org/).

are quite conservative, and the hCYB5B structure confirms our expectation that they would participate in interactions similar to those observed for Met23 and Ile32 in the rCYB5B hydrophobic cluster (Figure 3A,C). The hCYB5B structure also confirms our prediction that the solvent-exposed side chain of Leu18 would engage in more extensive hydrophobic interactions than are possible for Ala18 in rCYB5B. The Leu18 side chain makes van der Waals contact with the side chains of both Leu47 and Leu36, whereas Ala18 in rCYB5A has only hydrophobic contact with the side chain of Leu47.

Residues 21 and 50 Extend the Hydrophobic Cluster. The stretch of polypeptide comprising residues 15−20 separates α1 and β4 and is herein termed the α1−β4 loop. In actuality, residues 17−20 constitute a type I β-turn. In the rCYB5B structure, the backbone CO group of Thr17 forms an H-bond with the side chain hydroxyl of Thr21, the first residue in β4 (Figure 3B). This hydrogen bond is apparently quite strong (O−O distance of 2.9 Å), consistent with the fact that the Thr21 side chain is completely excluded from solvent (see Figure S4 of the Supporting Information). In addition, the Thr21 γ-CH_3 group makes van der Waals contact with one of the γ-CH_3 groups of Leu47 (C−C distance of 4.4 Å) and with the β-CH_3 group of invariant cytochrome b_5 residue Ala50 (C−C distance of 3.4 Å) (Figure 3A). Thr21 and Ala50 thereby extend the hydrophobic cluster described above for rCYB5B. Residue 21 is also Thr in all known examples of mammalian CYB5A. In the structure of the bCYB5A lipase fragment, interactions involving the Thr21 side chains are virtually identical to those described above for rCYB5B.[10] However, in the more recently determined structure of the bCYB5A tryptic fragment (PDB entry 1EHB), the α1−β4 loop adopts an alternate conformation in which this interaction is absent and the Thr21 side chain forms H-bonds to two water molecules. This is consistent with very high *B* factors for the α1−β4 loop in the lipase fragment structure,[10] which indicate that it has unusually high dynamic mobility.

Leu21 in hCYB5B Alters β4−β5 Interactions Relative to Those in rCYB5B. As noted above, residue 21 in CYB5A is an invariant Thr and is also Thr in rCYB5B. Only two other known mammalian CYB5B proteins, from mouse and opossum, contain Thr21 (Figure S1 of the Supporting Information). In hCYB5B and other primate CYB5B proteins, residue 21 is Leu. It is also Leu in the rabbit and pig proteins and is Ile in the proteins from horse, dog, cow, and panda. Like Thr21 in rCYB5B, Leu21 in the hCYB5B structure is fully excluded from solvent (Figure S4 of the Supporting Information). As shown in Figure 3, however, the bulky hydrophobic side chain of Leu21 in hCYB5B leads to several distinct differences in interactions relative to those of Thr21 in rCYB5B. First, it precludes side chain H-bond interactions with any residues within the α1−β4 loop (or with water if the loop adopts an open conformation as in PDB entry 1EHB). Second, it extends the hydrophobic cluster described above for rCYB5B, because the Leu21 side chain in hCYB5B

dx.doi.org/10.1021/bi2004729 |*Biochemistry* 2011, 50, 5544–5554

Table 1. Average Backbone rmsd, rmsf, and Heme SASA Values from the Three CYB5B Simulations

	rmsd (Å)		rmsf (Å)		SASA (Å^2)
simulation	chain[a]	heme	chain[a]	heme	heme
rCYB5B	0.6	0.7	1.0	0.8	241.66 ± 17.83 (221.7)[b]
hCYB5 (1)[c]	0.5	0.6	0.9	0.9	243.16 ± 18.11 (217.6)[b]
hCYB5 (2)[d]	0.9	0.7	1.1	0.9	243.22 ± 17.01

[a] Backbone (Cα, C, and N) atoms of amino acid residues 4−84. [b] Heme SASA calculated from X-ray crystal structures. [c] Including WAT11 and WAT194. [d] WAT11 and WAT194 removed prior to simulation.

makes van der Waals contact not only with the side chains of Leu47 and Ala50 but also with those of Leu23 and Leu36 (Figure 3C). Third, the greater bulk of the Leu21 side chain in hCYB5B results in displacement of the Ala50 β-methyl group by approximately 2.5 Å relative to its location in rCYB5B (Figure 3). The backbones of residues 51−53 in β5 are displaced to similar extents (Figure 3 and Figure S3B of the Supporting Information).

The movement of residues 50−53 needed to accommodate Leu at position 21 in hCYB5B is accompanied by the loss of two of the three hydrogen bonds between β4 and β5 (Figure 3D and Figure S5B of the Supporting Information), specifically those between the α-CO group of Trp22 in β4 and the α-NH group of Gly51 in β5, and between the α-NH group of Val24 in β4 and the α-CO group of Val52 in β5. Hydrogen bonding between those residues in strands β4 and β5 of hCYB5B is instead mediated by two water molecules [WAT11 and WAT194, respectively (Figure 3D)] that are completely excluded from contact with bulk solvent (solvent accessible surface area of 0.00 Å^2).[51] WAT11 has two additional possible H-bond acceptors, the α-CO group of Arg15 (O−O distance of 3.1 Å) and the α-CO group of Val12 (O−O distance of 3.0 Å), while WAT194 has one (the α-CO group of Gln49, with an O−O distance of 2.7 Å). We find no evidence of a second H-bond donating partner for either water molecule. In addition, the water molecules are too far apart (O−O distance of 4.9 Å) to permit a water−water H-bond. The *B* factors for WAT11 and WAT194 are 13.3 and 16.5, respectively, well below the average *B* factor for water molecules in the crystal structure (34.4) but remarkably similar to the average *B* factors of main chain atoms of their protein hydrogen bonding partners (12.2). In addition, the hydrogen bonds between the buried water molecules and the protein are quite short (Figure S5B of the Supporting Information). Both of these observations are suggestive of strong hydrogen bonding interactions.

A statistical study of protein crystal structures has shown that more than 90% of buried water molecules in proteins are associated with large internal cavities.[52] A more recent statistical study involving a much larger database has further revealed that well-resolved internal water molecules strongly prefer to form hydrogen bonds with residues that are not involved in α-helical or β-sheet secondary structures.[53] They also commonly bridge interactions between proteins and their ligands.[54] Water molecules that reside between strands of β-sheets, as in the hCYB5B crystal structure, appear to be quite rare. One well-known example is a highly conserved, fully buried water molecule located within a β-bulge in lectins.[55] Conserved internal water molecules bridging H-bonds between residues at the termini of β-strands, observed in trypsin, have been suggested to resemble intermediates in β-sheet formation during protein folding.[56]

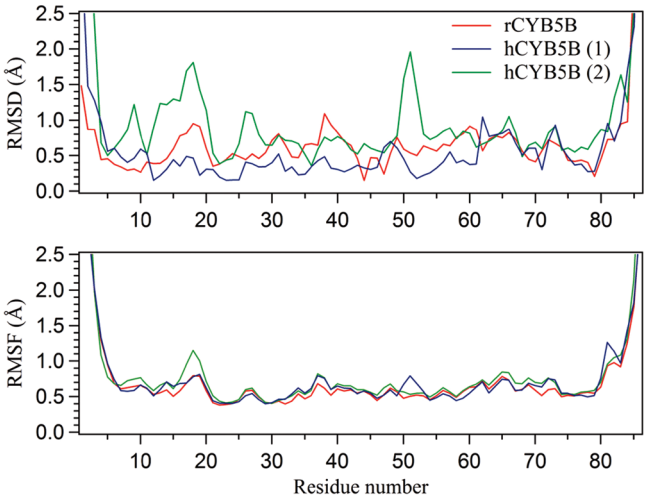

Figure 4. Backbone (Cα) root-mean-square deviation (top) and fluctuation (bottom) plots of the average trajectory structures vs the starting X-ray coordinates for the three MD simulations.

WAT11 in the hCYB5B Simulation Exchanges with Bulk Solvent. As an approach to comparing solution properties of rCYB5B and hCYB5B and to elucidating possible roles of the buried water molecules in the hCYB5B crystal structure, we performed 10 ns molecular dynamics (MD) simulations. We first discuss simulations comparing rCYB5B and hCYB5B in which WAT11 and WAT194 are present in their crystallographically determined locations. No other water molecules of crystallization were included in the simulations. Average root-mean-square deviation (rmsd) and fluctuation (rmsf) values for the heme and the polypeptide (Table 1) are less than 1.1 Å in the two simulations, indicating little deviation from the respective starting experimental coordinates. The individual amino acid residue rmsd plots in Figure 4 (top panel) likewise show essentially no deviation from the starting coordinates for rCYB5B and for hCYB5B, and the corresponding RMSF plots in Figure 4 (bottom panel) reveal the absence of significant mobility during the simulations in the MD trajectories.

Visual inspection of the hCYB5B MD trajectory showed that WAT194 remained close to its original location for the full 10 ns, with hydrogen bonds to Val24 and Val52 and occasionally to one of the other buried water molecules. WAT11 was considerably more mobile and exited the protein after 4.1 ns. The MD trajectories were subsequently examined to identify all bulk water molecules that approached within 4.5 Å of Trp22, Val24, Gly51, or Val52 during the simulation. Among the 23 molecules so identified, four were observed to occupy the space between β4 and β5 at some point during the simulation or to be otherwise involved with the water exchange mechanism. Three exchanges of a buried water molecule with a bulk water molecule were observed during the simulation, each occurring via an intermediate structure containing three buried water molecules. None of the water entry or exit events involved significant backbone or side chain conformational changes.

Two distinct sites for water entry and exit were identified. The first water exchange event, which involves both of these sites, is illustrated in Figure 5. Within 0.27 ns, bulk water molecule wat1877 (red sphere) has docked to the protein, forming H-bonds with the backbone C═O group of Ala13 (located in helix α1) and the side chain amide group of Asn16 (located in the

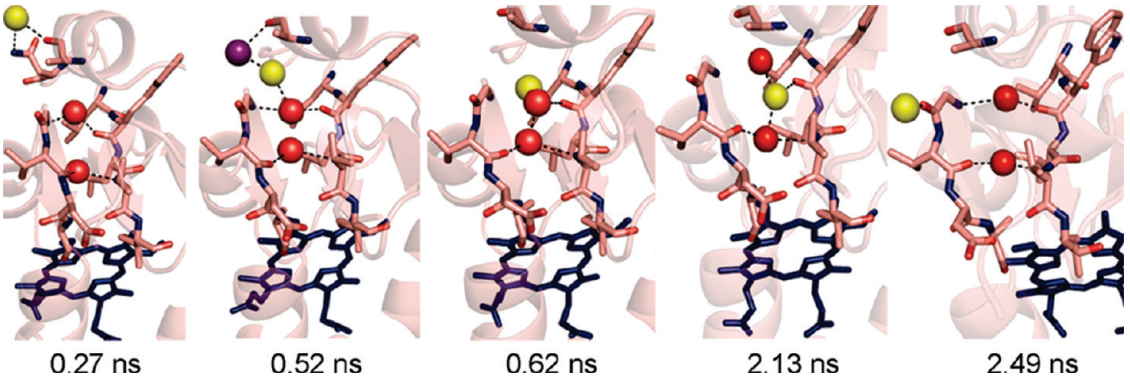

Figure 5. Location of water molecules at various time points in the 10 ns MD simulation of hCYB5B. The waters of crystallization (WAT11 and WAT194) are shown as red spheres; bulk solvent wat1877 is shown as a yellow sphere, and bulk solvent wat4142 is shown as a purple sphere (wat1877 and wat4142 arise from the water box created for the simulations). Hydrogen bonds are represented as black dashes. Please refer to the text for details. The image was generated using PyMol version 0.99 (http://www.pymol.org/).

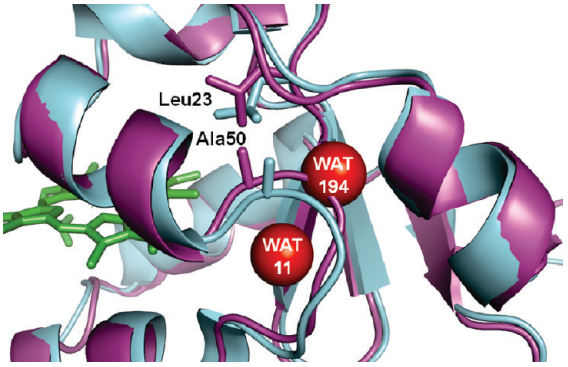

Figure 6. Overlay of molecule A from the hCYB5B crystal structure (cyan) with a representative structure from the 10 ns MD simulation of hCYB5B performed without WAT11 and WAT194 (magenta). The polypeptide backbones are represented in cartoon mode, and heme (green) and the side chains of Leu21 and Ala51 in each protein are represented as sticks. WAT11 and WAT194 from the hCYB5B crystal structure are represented as red spheres. The image was generated using PyMol version 0.99 (http://www.pymol.org/).

α1−β4 loop). Notably, this water molecule replicates nearly exactly the location and interactions exhibited by WAT121 in the hCYB5B crystal structure (see Figure 3D). The wat1877 molecule enters the protein interior between β4 and β5, via hydrogen bonding with WAT11 and a second bulk water molecule (wat4142, yellow sphere), which replaces it at the entry site. WAT11 and wat1877 subsequently trade places as WAT11 is pushed in the direction of, but not through, the second water entry−exit site. This sequence of events is then essentially repeated, with WAT11 moving toward WAT194 and pushing wat1877 toward, and through, the second entry−exit site. Exit of wat1877 from the protein involves the formation of a hydrogen bond with the backbone C═O group of Gly51 and with bulk solvent.

The Buried Water Molecules May Not Be Required for Maintenance of the hCYB5B Fold. We also performed a simulation of hCYB5B in which WAT11 and WAT194 were initially removed, along with all other waters of crystallization. In this simulation, small but significant localized deviations from the starting coordinates were observed, most notably for residues 50−52 (Figure 4A). Visual inspection of the trajectory for that simulation revealed that the change is due to formation of hydrogen bonds between Val24 and Val52, and between Trp22 and Gly51. The hydrogen bonds, which form during the preproduction equilibration step, are virtually identical to those observed between β4 and β5 in the rCYB5B crystal structure and MD simulation. They remain intact throughout the 10 ns simulation, as shown by the low rmsf values for the corresponding residues (Figure 4B). Figure 4A also reveals significant backbone deviation for residues 15−19 in the conformationally mobile α1−β4 loop, with maximal displacement at Leu18. This deviation can be attributed to movement of the Ala50 side chain deeper into the protein interior as the β4−β5 hydrogen bonds form, and consequent reorganization of the Leu21 side chain to prevent a steric clash (Figure 6). In the hCYB5B crystal structure, the Leu21 side chain adopts the second most common conformation (34% of total) observed for Leu residues in β-sheets [$\chi_1 = 178°$, and $\chi_2 = 65°$ (tp using the convention of Lovell et al.[57])]. After the structural change, the Leu21 side chain is in a conformation observed for only 3% of Leu residues in β-sheets (tt, where $\chi_1 = -160°$ and $\chi_2 = 169°$). This suggests that normal hydrogen bonding interactions between β4 and β5 in hCYB5B introduce strain.

The Redox Potentials of rCYB5B and hCYB5B Are Very Similar. Type A b_5 cytochromes have been found to exhibit similar redox potentials [0 ± 10 mV (all reported potentials vs SHE)],[58−61] consistent with their highly conserved amino acid sequences. Reported redox potentials for rCYB5B (−102 mV)[22] and hCYB5B (−40 mV)[28] are more negative, suggesting a need for a stronger electron delivery driving force.[28] The significant difference in the reported redox potentials for rCYB5B and hCYB5B is suggestive of differences in the heme environment.[62] However, our MD simulation data reveal that there is virtually no difference in average heme solvent exposure in the two proteins (Table 1). Furthermore, there is no difference in the number and type of charged residues in their heme-binding pockets.

To firmly establish whether structural divergence of hCYB5B and rCYB5B has been accompanied by divergence of their redox potentials, we decided to perform new side-by-side studies. The tryptic fragment of bCYB5A (residues 4−82) was included in the study for the purpose of comparison. We opted to utilize redox potentiometry[63] rather than voltammetry, as the latter requires the use of agents to facilitate protein−electrode interactions,[64] which is known to influence measured cytochrome b_5 redox

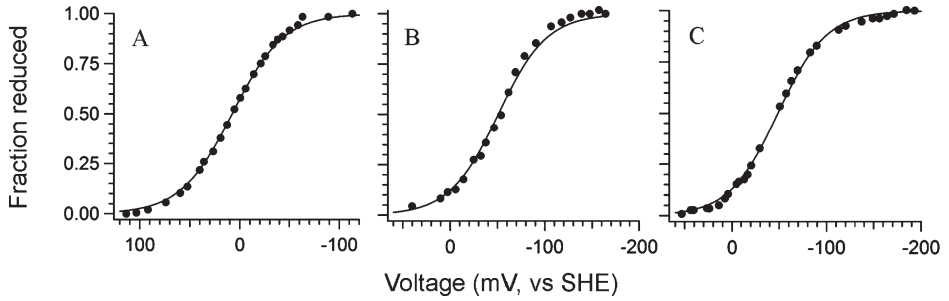

Figure 7. Representative plots of redox titration data for bCYB5A (A), rCYB5B (B), and hCYB5B (C), with fits to the one-electron Nernst equation. Redox potentials are listed in Table 2.

Table 2. Data from Redox Potentiometry Experiments

	bCYB5A	rCYB5B	hCYB5B
$E^{o\prime}$ (mV vs SHE)	5.5 ± 1.8	−54.8 ± 1.3	−53.8 ± 1.2

potentials.[22,65] The apparatus used in our experiments was housed in a glovebox to minimize adventitious oxygen, which can lead to erroneous redox potential measurements by preventing equilibrium from being established.[63] Representative spectra from the redox titrations are shown in Figure S6 of the Supporting Information, and corresponding data plots with fits to the one-electron Nernst equation appear in Figure 7. Formal reduction potentials obtained from the fits, all referenced to the standard hydrogen electrode (SHE), are compiled in Table 2.

The redox potential obtained for the bCYB5A tryptic fragment is close to the average value of redox potentials determined independently for the same protein at pH 7, 24−25 °C, and an ionic strength of ∼0.1 M by redox potentiometry (13 mV)[66] and by spectroelectrochemistry using an optically transparent thin layer electrode (OTTLE) (5 mV[67] and −1.9 mV[61]). The hCYB5B redox potential determined in this work is ∼15 mV more negative than the previously reported one, obtained using an apparatus similar to the one employed here but in which an inert atmosphere was achieved without use of a glovebox.[28] On the other hand, the rCYB5B redox potential determined in this study is considerably less negative than the previously reported value[22] determined using an OTTLE. In fact, the redox potentials of rCYB5B and hCYB5B determined in this work are virtually identical (approximately −55 mV).

The apparent discrepancy between the rCYB5B redox potential reported herein and the previously published value may relate to the unusual sensitivity of the cytochrome b_5 oxidation−reduction equilibrium to experimental conditions[67] and even to methodology.[58] Regardless of its source, we are confident that the redox potentials determined in this study for bCYB5A, rCYB5B, and hCYB5B are valid for the stated conditions. Support for this conjecture is provided by the fact that cyclic voltammetry data for bCYB5A and rCYB5B recorded in the presence of varying concentrations of divalent metal ions revealed a constant ∼70 mV redox potential difference.[22] This is nearly the same as the difference obtained in our work (∼60 mV).

Ala54 in β5 May Play a Key Role in Stabilizing the Cytochrome b_5 Fold. The structural consequences of the release of heme from cytochrome b_5 were first demonstrated in solution NMR studies of the heme-free (apo) form of rat CYB5A.[68,69] The core 1 helices α2−α5 unfold, consistent with their very low helix propensities,[70] and β5 dissociates from β4. In contrast, core 2 retains a nativelike fold. Subsequent studies have indicated that similar changes occur upon loss of heme from CYB5B.[25,26] Release of heme from cytochrome b_5 can conceivably occur via several pathways, all of which require dissociation of both His−Fe bonds. Available evidence suggests that the bond involving His39 is the first to rupture.[49,71] His−Fe bond dissociation by itself could be a triggering event for heme release, as it would result in melting of the adjacent core 1 helices. A more likely possibility, suggested by NMR studies, is that heme release is promoted by conformational fluctuations in the core 1 polypeptide. For example, it has been demonstrated that conformational mobility is greater in the ferric form of CYB5A than in the more stable ferrous form.[18,72] In addition, core 1 is much more dynamic in the ferric form of CYB5A than in the ferric form of the more stable CYB5B.[49]

Core 1 conformational changes facilitating the release of heme from cytochrome b_5 could potentially begin in the vicinity of β5, as suggested by two independent MD simulations of bCYB5A. Both simulations revealed formation of a large surface cleft resulting from a conformational change,[23,73] which included loss of the hydrogen bond between Gly51 in β5 and Trp22 in β4.[23] Complete separation of β5 from β4 would favor unfolding of adjacent core 1 helices α3 and α4 with consequent weakening of the His39−Fe and His63−Fe bonds, respectively. In the hCYB5B structure, two of the three H-bonds holding β4 and β5 together are already mediated by water molecules. The MD simulation data presented herein indicate that an additional water molecule can reversibly enter core 1 of hCYB5B, yielding intermediates containing three buried water molecules between β5 and β4. Complete separation of β5 from β4 would result if one of the three buried water molecules in such an intermediate were to shift position and insert between the backbones of Ala54 and Val24. Examination of CYB5B and CYB5A structures suggested to us that this may be difficult, because of the participation of Ala54 in at least two additional key interactions that would likely be compromised if the H-bond between Ala54 and residue 24 in β4 is broken to accommodate a bridging water molecule. First, the methyl side chain of Ala54 extends the CYB5B hydrophobic patch (and the less extensive CYB5A patch) by packing against the side chain of residue 23 as well as with heme. In addition, the Ala54 α-CO group forms an H-bond with the α-NH group of invariant residue Phe58, located in α4 and also part of the CYB5B and CYB5A hydrophobic patches. As shown in Figure 3, the Phe58 side chain engages in face-to-face stacking with heme ligand His63 and edge-to-face stacking with heme. Notably, Ala54 and Phe58 have two of the most protected backbone α-NH groups in core 1 of CYB5B and CYB5A as evidenced in H−D exchange studies monitored by NMR.[18,49] This indicates that once the Ala54 and Phe58

backbone NH groups are accessible to solvent, most if not all of the other core 1 backbone amides are as well, which would occur upon core 1 unfolding leading to heme release.

CONCLUDING REMARKS

The cytochrome b_5 fold has been termed an adaptable module because of its ability to accommodate a wide variety of insertions, deletions, and mutations.[74] Herein we have reported a new example of this adaptability, namely accommodation of a nonconservative internal mutation (Thr21 in rCYB5B to Leu21 in hCYB5B) by burial of two to three water molecules between β-sheet strands β5 and β4. Molecular dynamics simulations indicate that one of the two buried water molecules in hCYB5B exchanges readily with bulk solvent. They also show that β5 and β4 can form normal hydrogen bonding interactions in hCYB5B if the buried water molecules are absent, but only if the Leu21 side chain adopts a rare (and likely strained) conformation. Regardless of whether the buried water molecules are an integral part of the hCYB5B structure in solution, these results strongly suggest that water more readily inserts between β5 and β4 in hCYB5B than in rCYB5B. This is interesting in light of the previously established fact that hCYB5B and rCYB5B exhibit nearly identical stability properties.[28] Perhaps the more extensive core 1 hydrophobic packing in hCYB5B in comparison to rCYB5B, resulting in large part from the presence of Leu rather than Thr at position 21, compensates for weakened $\beta5-\beta4$ interactions resulting from the same nonconservative mutation. Such an interpretation is consistent with our studies showing that the greater stability exhibited by rCYB5B in comparison to that of bCYB5A is due to more extensive hydrophobic packing in core 1.[23−25] The fact that two of three hydrogen bonds between β5 and β4 can be compromised without adversely affecting hCYB5B stability suggests that the third H-bond (between Ala54 in β5 and Val24 in β4) plays a dominant role in maintaining the hCYB5B fold. In fact, this may be the case in all b_5 cytochromes.

Another important conclusion from this work is that the redox potentials of hCYB5B and rCYB5B are virtually identical and ~60 mV more negative than those reported herein and elsewhere for CYB5A. The experimental conditions and methodology used in this study were chosen because they minimize interactions of the proteins with materials that could influence the measured redox potentials.[67,75] The redox potentials of type A and type B b_5 cytochromes may very well deviate from the values obtained herein when the proteins are in their native environments and functionally interacting with their redox partners.[75]

Similarity of mammalian CYB5A redox potentials is not surprising in light of their high degree of amino acid sequence conservation, particularly among residues defining the heme-binding pocket. The results presented herein indicate that mammalian type B b_5 cytochromes also exhibit a narrow range of redox potentials, despite much greater amino acid sequence diversity as exemplified by rCYB5B and hCYB5B. Current efforts in our laboratories are directed toward delineating the structural factors responsible for the more negative redox potentials exhibited by CYB5B relative to CYB5A.

ASSOCIATED CONTENT

Supporting Information. Additional data. This material is available free of charge via the Internet at http://pubs.acs.org.

AUTHOR INFORMATION

Corresponding Author

*Department of Chemistry, University of Kansas, Lawrence, KS 66045. Phone: (785) 864-4090. Fax: (785) 864-5396. E-mail: drb@ku.edu.

Funding Sources

This work was supported by a grant from the National Science Foundation (MCB-0446326, to M.R. and D.R.B.) and by the Departments of Chemistry and Molecular Biosciences of the University of Kansas.

ACKNOWLEDGMENT

We thank Prof. Emily Scott for use of her FPLC system and Dr. Scott Lovell for helpful discussions of the crystallographic data.

ABBREVIATIONS

CYB5A, type A cytochrome b_5; CYB5B, type B cytochrome b_5; bCYB5A, bovine CYB5A; rCYB5B, rat CYB5B; hCYB5B, human CYB5B; MD, molecular dynamics; rmsd, root-mean-square deviation; PDB, Protein Data Bank; rmsf, root-mean-square fluctuation; SHE, standard hydrogen electrode.

REFERENCES

(1) Kuroda, R., Ikenoue, T., Honsho, M., Tsujimoto, S., Mitoma, J., and Ito, A. (1998) Charged amino acids at the carboxy-terminal portions determine the intracellular locations of two isoforms of cytochrome b_5. *J. Biol. Chem. 273*, 31097–31102.

(2) Lederer, F., Ghrir, R., Guiard, B., Cortial, S., and Ito, A. (1983) Two homologous cytochromes b_5 in a single cell. *Eur. J. Biochem. 132*, 95–102.

(3) Schenkman, J. B., and Jansson, I. (2003) The many roles of cytochrome b_5. *Pharmacol. Ther. 97*, 139.

(4) Vergeres, G., and Waskell, L. (1995) Cytochrome b_5, its functions, structure and membrane topology. *Biochimie 77*, 604–620.

(5) Finn, R., McLaughlin, L., Hughes, C., Song, C., Henderson, C., and Roland Wolf, C. (2010) Cytochrome b_5 null mouse: A new model for studying inherited skin disorders and the role of unsaturated fatty acids in normal homeostasis. *Transgenic Res.*, 1–12.

(6) McLaughlin, L. A., Ronseaux, S., Finn, R. D., Henderson, C. J., and Roland Wolf, C. (2010) Deletion of microsomal cytochrome b_5 profoundly affects hepatic and extrahepatic drug metabolism. *Mol. Pharmacol. 78*, 269–278.

(7) Ito, A., Hayashi, S.-i., and Yoshida, T. (1981) Participation of a cytochrome b_5-like hemoprotein of outer mitochondrial membrane (OM cytochrome b) in NADH-semidehydroascorbic acid reductase activity of rat liver. *Biochem. Biophys. Res. Commun. 101*, 591–598.

(8) Ogishima, T., Kinoshita, J.-y., Mitani, F., Suematsu, M., and Ito, A. (2003) Identification of outer mitochondrial membrane cytochrome b_5 as a modulator for androgen synthesis in Leydig cells. *J. Biol. Chem. 278*, 21204–21211.

(9) Murphy, D., Parker, J., Zhou, M. L., Fadlelmola, F. M., Steidl, C., Karsan, A., Gascoyne, R. D., Chen, H., and Banerjee, D. (2010) Constitutively overexpressed 21 kDa protein in Hodgkin lymphoma and aggressive non-Hodgkin lymphomas identified as cytochrome B-5b (CYB5B). *Mol. Cancer 9*, 14.

(10) Durley, R. C. E., and Mathews, F. S. (1996) Refinement and structural analysis of bovine cytochrome b_5 at 1.5 Å resolution. *Acta Crystallogr. D52*, 65–76.

(11) Wu, J., Gan, J.-H., Xia, Z.-X., Wang, Y.-H., Wang, W.-H., Xue, L.-L., Xie, Y., and Huang, Z.-X. (2000) Crystal structure of recombinant trypsin-solubilized fragment of cytochrome b_5 and the structural comparison with Val61His mutant. *Proteins: Struct., Funct., Genet. 40*, 249–257.

(12) Rodriguez-Maranon, M. J., Qiu, F., Stark, R. E., White, S. P., Zhang, X., Foundling, S. I., Rodriguez, V., Schilling, C. L., III, Bunce, R. A., and Rivera, M. (1996) ^{13}C NMR spectroscopic and X-ray crystallographic study of the role played by mitochondrial cytochrome b_5 heme propionates in the electrostatic binding to cytochrome c. *Biochemistry 35*, 16378–16390.

(13) Mathews, F. S., Levine, M., and Argos, P. (1971) Structure of calf liver cytochrome b_5 at 2.8 A resolution. *Nat. New Biol. 233*, 15–16.

(14) Mathews, F. S., Levine, M., and Argos, P. (1972) Three-dimensional Fourier synthesis of calf liver cytochrome b_5 at 2.8 Å resolution. *J. Mol. Biol. 64*, 449–464.

(15) Mathews, F. S., Gerwinsky, E. W., and Argos, P. (1979) The X-ray crystallographic structure of calf liver cytochrome b_5. In *The Porphyrins* (Dolphin, D., Ed.) pp 107−147, Academic Press, New York.

(16) Zhang, Q., Cao, C., Wang, Z.-Q., Wang, Y.-H., Wu, H., and Huang, Z.-X. (2004) The comparative study on the solution structures of the oxidized bovine microsomal cytochrome b_5 and mutant V45H. *Protein Sci. 13*, 2161–2169.

(17) Muskett, F. W., Kelly, G. P., and Whitford, D. (1996) The solution structure of bovine ferricytochrome b_5 determined using heteronuclear NMR methods. *J. Mol. Biol. 258*, 172–189.

(18) Arnesano, F., Banci, L., Bertini, I., and Felli, I. C. (1998) The solution structure of oxidized rat microsomal cytochrome b_5. *Biochemistry 37*, 173–184.

(19) Banci, L., Bertini, I., Rosato, A., and Scacchieri, S. (2000) Solution structure of oxidized microsomal rabbit cytochrome b_5. *Eur. J. Biochem. 267*, 755–766.

(20) Nunez, M., Guittet, E., Pompon, D., van Heijenoort, C., and Truan, G. (2010) NMR structure note: Oxidized microsomal human cytochrome b5. *J. Biomol. NMR 47*, 289–295.

(21) Silchenko, S., Sippel, M. L., Kuchment, O., Benson, D. R., Mauk, A. G., Altuve, A., and Rivera, M. (2000) Hemin is kinetically trapped in cytochrome b_5 from rat outer mitochondrial membrane. *Biochem. Biophys. Res. Commun. 271*, 467–472.

(22) Rivera, M., Wells, M. A., and Walker, F. A. (1994) Cation-promoted cyclic voltammetry of recombinant rat outer mitochondrial membrane cytochrome b_5 at a gold electrode modified with β-mercaptopropionic acid. *Biochemistry 33*, 2161–2170.

(23) Altuve, A., Silchenko, S., Lee, K.-H., Kuczera, K., Terzyan, S., Zhang, X., Benson, D. R., and Rivera, M. (2001) Probing the differences between rat liver outer mitochondrial membrane cytochrome b_5 and microsomal cytochromes b_5. *Biochemistry 40*, 9469–9483.

(24) Cowley, A. B., Altuve, A., Kuchment, O., Terzyan, S., Zhang, X., Rivera, M., and Benson, D. R. (2002) Toward engineering the stability and hemin binding properties of microsomal cytochromes b_5 into rat outer mitochondrial membrane cytochrome b_5: Examining the influence of residues 25 and 71. *Biochemistry 41*, 11566–11581.

(25) Cowley, A. B., Rivera, M., and Benson, D. R. (2004) Stabilizing roles of residual structure in the empty heme binding pockets and unfolded states of microsomal and mitochondrial apocytochrome b_5. *Protein Sci. 13*, 2316–2329.

(26) Cowley, A. B., Sun, N., Rivera, M., and Benson, D. R. (2005) Divergence in non-specific hydrophobic packing interactions in the apo state, and its possible role in functional specialization of mitochondrial and microsomal cytochrome b_5. *Biochemistry 44*, 14606–14615.

(27) Wang, L., Sun, N., Terzyan, S., Zhang, X., and Benson, D. R. (2006) A histidine/tryptophan π-stacking interaction stabilizes the heme-independent folding core of microsomal apocytochrome b_5 relative to that of mitochondrial apocytochrome b_5. *Biochemistry 45*, 13750–13759.

(28) Altuve, A., Wang, L., Benson, D. R., and Rivera, M. (2004) Mammalian mitochondrial and microsomal cytochromes b_5 exhibit divergent structural and biophysical characteristics. *Biochem. Biophys. Res. Commun. 314*, 602–609.

(29) Wang, L., Cowley, A. B., Terzyan, S., Zhang, X., and Benson, D. R. (2007) Comparison of cytochromes b_5 from insects and vertebrates. *Proteins 67*, 293–304.

(30) Rivera, M., Barillas-Mury, C., Christensen, K. A., Little, J. W., Wells, M. A., and Walker, F. A. (1992) Gene synthesis, bacterial expression, and ^{1}H NMR spectroscopic studies of the rat outer mitochondrial membrane cytochrome b_5. *Biochemistry 31*, 12233–12240.

(31) Otwinowski, Z., and Minor, W. (1997) Processing of X-ray diffraction data collected in oscillation mode. *Methods Enzymol. 276*, 307–326.

(32) Navaza, J. (1994) AMoRe: An automated package for molecular replacement. *Acta Crystallogr. A50*, 157–163.

(33) Brunger, A. T., Adams, P. D., Clore, G. M., DeLano, W. L., Gros, P., Grosse-Kunstleve, R. W., Jiang, J. S., Kuszewski, J., Nilges, M., and Pannu, N. S. (1998) Crystallography and NMR system: A new software suite for macromolecular structure determination. *Acta Crystallogr. D54*, 905–921.

(34) Roussel, A., and Cambillau, C. (1989) TURBO-FRODO. In *Silicon Graphics Geometry Partners Directory*, pp 77−79, Silicon Graphics, Mountain View, CA.

(35) Murshudov, G. N., Vagin, A. A., and Dodson, E. J. (1997) Refinement of macromolecular structures by the maximum-likelihood method. *Acta Crystallogr. D53*, 240–255.

(36) *SAINT: Software for the CCD Detector System*, version 4.035 (1995) Siemens Analytical Instruments Division, Madison, WI.

(37) Tronrud, D. E., Ten Eyck, L. F., and Matthews, B. W. (1987) An efficient general-purpose least-squares refinement program for macromolecular structures. *Acta Crystallogr. A43*, 489–501.

(38) Emsley, P., and Cowtan, K. (2004) Coot: Model-building tools for molecular graphics. *Acta Crystallogr. D60*, 2126–2132.

(39) Brooks, B. R., Brooks, C. L., III, Mackerell, A. D., Jr., Nilsson, L., Petrella, R. J., Roux, B., Won, Y., Archontis, G., Bartels, C., Boresch, S., Caflisch, A., Caves, L., Cui, Q., Dinner, A. R., Feig, M., Fischer, S., Gao, J., Hodoscek, M., Im, W., Kuczera, K., Lazaridis, T., Ma, J., Ovchinnikov, V., Paci, E., Pastor, R. W., Post, C. B., Pu, J. Z., Schaefer, M., Tidor, B., Venable, R. M., Woodcock, H. L., Wu, X., Yang, W., York, D. M., and Karplus, M. (2009) CHARMM: The biomolecular simulation program. *J. Comput. Chem. 30*, 1545–1614.

(40) Mackerell, A. D., Feig, M., and Brooks, C. L. (2004) Extending the treatment of backbone energetics in protein force fields: Limitations of gas-phase quantum mechanics in reproducing protein conformational distributions in molecular dynamics simulations. *J. Comput. Chem. 25*, 1400–1415.

(41) Brunger, A. T., and Karplus, M. (1988) Polar hydrogen positions in proteins: Empirical energy placement and neutron diffraction comparison. *Proteins: Struct., Funct., Genet. 4*, 148–156.

(42) Jo, S., Kim, T., Iyer, V. G., and Im, W. (2008) CHARMM-GUI: A web-based graphical user interface for CHARMM. *J. Comput. Chem. 29*, 1859–1865.

(43) Tildesley, D. J., and Allen, M. P. (1987) *Computer Simulations of Liquids*, Oxford Science Publications, London.

(44) Feller, S. E., Zhang, Y. H., Pastor, R. W., and Brooks, B. R. (1995) Constant-pressure molecular-dynamics simulation: The Langevin piston method. *J. Chem. Phys. 103*, 4613–4621.

(45) Essmann, U., Perera, L., Berkowitz, M. L., Darden, T., Lee, H., and Pedersen, L. G. (1995) A smooth particle mesh Ewald method. *J. Chem. Phys. 103*, 8577–8593.

(46) Ryckaert, J. P., Ciccotti, G., and Berendsen, H. J. C. (1977) Numerical-Integration of Cartesian Equations of Motion of a System with Constraints: Molecular Dynamics of N-Alkanes. *J. Comput. Phys. 23*, 327–341.

(47) Lee, B., and Richards, F. M. (1971) Interpretation of Protein Structures: Estimation of Static Accessibility. *J. Mol. Biol. 55*, 379–400.

(48) Humphrey, W., Dalke, A., and Schulten, K. (1996) VMD: Visual molecular dynamics. *J. Mol. Graphics 14*, 33–38.

(49) Simeonov, M., Altuve, A., Massiah, M. A., Wang, A., Eastman, M. A., Benson, D. R., and Rivera, M. (2005) Mitochondrial and microsomal ferric b_5 cytochromes exhibit divergent conformational plasticity in the context of a common fold. *Biochemistry 44*, 9308–9319.

(50) Sun, N., Wang, A., Cowley, A. B., Altuve, A., Rivera, M., and Benson, D. R. (2005) Enhancing the stability of microsomal cytochrome

b_5: A rational approach informed by comparative studies with the outer mitochondrial membrane isoform. *Protein Eng., Des. Sel. 18*, 571–579.

(51) Gerstein, M. (1992) A resolution-sensitive procedure for comparing protein surfaces and its application to the comparison of antigen-combining sites. *Acta Crystallogr. A48*, 271–276.

(52) Williams, M. A., Goodfellow, J. M., and Thornton, J. M. (1994) Buried waters and internal cavities in monomeric proteins. *Protein Sci. 3*, 1224–1235.

(53) Park, S., and Saven, J. G. (2005) Statistical and molecular dynamics studies of buried waters in globular proteins. *Proteins: Struct., Funct., Bioinf. 60*, 450–463.

(54) Lu, Y., Wang, R., Yang, C.-Y., and Wang, S. (2007) Analysis of Ligand-Bound Water Molecules in High-Resolution Crystal Structures of Protein−Ligand Complexes. *J. Chem. Inf. Model. 47*, 668–675.

(55) Loris, R., Stas, P. P., and Wyns, L. (1994) Conserved waters in legume lectin crystal structures. The importance of bound water for the sequence-structure relationship within the legume lectin family. *J. Biol. Chem. 269*, 26722–26733.

(56) Finer-Moore, J. S., Kossiakoff, A. A., Hurley, J. H., Earnest, T., and Stroud, R. M. (1992) Solvent structure in crystals of trypsin determined by X-ray and neutron diffraction. *Proteins: Struct., Funct., Bioinf. 12*, 203–222.

(57) Lovell, S. C., Word, J. M., Richardson, J. S., and Richardson, D. C. (2000) The penultimate rotamer library. *Proteins: Struct., Funct., Bioinf. 40*, 389–408.

(58) Aono, T., Sakamoto, Y., Miura, M., Takeuchi, F., Hori, H., and Tsubaki, M. (2010) Direct electrochemical analyses of human cytochromes b5 with a mutated heme pocket showed a good correlation between their midpoint and half wave potentials. *J. Biomed. Sci. 17*, 90.

(59) Martinis, S. A., Sotiriou, C., Chang, C. K., and Sligar, S. G. (1989) Characterization of cytochrome b5 reconstituted with a ferric chlorin and a ferric oxochlorin. *Biochemistry 28*, 879–884.

(60) Funk, W. D., Lo, T. P., Mauk, M. R., Brayer, G. D., MacGillivray, R. T. A., and Mauk, A. G. (1990) Mutagenic, electrochemical, and crystallographic investigation of the cytochrome b_5 oxidation-reduction equilibrium: Involvement of asparagine-57, serine-64, and heme propionate-7. *Biochemistry 29*, 5500–5508.

(61) Walker, F. A., Emrick, D., Rivera, J. E., Hanquet, B. J., and Buttlaire, D. H. (1988) Effect of heme orientation on the reduction potential of cytochrome b_5. *J. Am. Chem. Soc. 110*, 6234–6240.

(62) Reedy, C. J., and Gibney, B. R. (2004) Heme protein assemblies. *Chem. Rev. 104*, 617–650.

(63) Dutton, P. L. (1978) Redox potentiometry: Determination of midpoint potentials of oxidation-reduction components of biological electron-transfer systems. *Methods Enzymol. 54*, 411–435.

(64) Armstrong, F. A., Cox, P. A., Hill, H. A., Lowe, V. J., and Oliver, B. N. (1987) Metal ions and complexes as modulators of protein-interfacial electron transport at graphite electrodes. *J. Electroanal. Chem. 217*, 331–366.

(65) Rivera, M., Seetharaman, R., Girdhar, D., Wirtz, M., Zhang, X., Wang, X., and White, S. (1998) The reduction potential of cytochrome b_5 is modified by its exposed heme edge. *Biochemistry 37*, 1485–1494.

(66) Iyanagi, T. (1977) Redox properties of microsomal reduced nicotinamide adenine dinucleotide-cytochrome b_5 reductase and cytochrome b_5. *Biochemistry 16*, 2725–2730.

(67) Reid, L. S., Taniguchi, V. T., Gray, H. B., and Mauk, A. G. (1982) Oxidation-reduction equilibrium of cytochrome b_5. *J. Am. Chem. Soc. 104*, 7516–7519.

(68) Falzone, C. J., Mayer, M. R., Whiteman, E. L., Moore, C. D., and Lecomte, J. T. J. (1996) Design challenges for hemoproteins: The solution structure of apocytochrome b_5. *Biochemistry 35*, 6519–6526.

(69) Falzone, C. J., Wang, Y., Vu, B. C., Scott, N. L., Bhattacharya, S., and Lecomte, J. T. J. (2001) Structural and dynamic perturbations induced by heme binding in cytochrome b_5. *Biochemistry 40*, 4879–4891.

(70) Davis, R. B., and Lecomte, J. T. J. (2008) Structural propensities in the heme binding region of apocytochrome b5. I. Free peptides. *Pept. Sci. 90*, 544–555.

(71) Ihara, M., Takahashi, S., Ishimori, K., and Morishima, I. (2000) Functions of fluctuations in the heme-binding loops of cytochrome b_5 revealed in the process of heme incorporation. *Biochemistry 39*, 5961–5970.

(72) Dangi, B., Sarma, S., Yan, C., Banville, D. L., and Guiles, R. D. (1998) The origin of differences in the physical properties of the equilibrium forms of cytochrome b_5 revealed through high-resolution NMR structures and backbone dynamic analyses. *Biochemistry 37*, 8289–8302.

(73) Storch, E. M., and Daggett, V. (1995) Molecular dynamics simulation of cytochrome b_5: Implications for protein-protein recognition. *Biochemistry 34*, 9682.

(74) Lederer, F. (1994) The cytochrome b_5-fold: An adaptable module. *Biochimie 76*, 674–692.

(75) Wirtz, M., Oganesyan, V., Zhang, X., Studer, J., and Rivera, M. (2000) Modulation of redox potential in electron transfer proteins: Effects of complex formation on the active site microenvironment of cytochrome b5. *Faraday Discuss.* 221–234, 257−268 (discussion).